






Bound states in the continuum in a waveguide structure covered by a two-dimensional square array of gold nanodisks

Sergey I. Pavlov ^{1,*}, Ilia M. Fradkin ², Sergey A. Dyakov ², Nikolay A. Feoktistov,¹ Alexey V. Nashchekin ¹,
and Alexander B. Pevtsov ¹

¹*Ioffe Institute, 194021 St Petersburg, Russia*

²*Skolkovo Institute of Science and Technology, 143025 Moscow, Russia*



(Received 3 July 2023; revised 14 September 2023; accepted 3 November 2023; published 27 November 2023)

A bound state in the continuum (BIC) is a concept of a wave phenomenon that remains confined even though it coexists with a continuous radiative spectrum. In photonics, such states are promising for the enhancement of the light-matter interaction. In this work, we study the optical properties of the $a\text{-Si}_{0.65}\text{C}_{0.35}\text{:H}$ -based planar waveguide structure covered by a two-dimensional array of gold nanodisks. To obtain BICs, we use a square lattice of nanodisks, which has one of the highest degrees of symmetry. The lattice provides light coupling to both TE and TM guided modes, while the single nanodisk supports localized plasmon resonance. We show that the structure possesses different types of BICs which are the result of the interaction of guided modes and single-particle resonances.

DOI: [10.1103/PhysRevB.108.205425](https://doi.org/10.1103/PhysRevB.108.205425)

I. INTRODUCTION

Periodic nanostructures are of great interest in the different fields of photonic applications because of their resonant properties, which can be adjusted by their geometry. A wide variety of optical resonances offers ample opportunities to manipulate light at the nanoscale [1]. Among others, plasmonic resonances [2,3], surface lattice resonances [4–7], and quasiguided resonances [8,9] either in one- and two-dimensional periodic structures are known, each with its own unique advantages.

In the past decades special resonant states, namely bound states in the continuum (BICs), have been extensively investigated [10,11]. BIC is, by definition, a perfectly confined state with eigenvalue that lies in the continuous spectrum of radiating waves; thus its Q factor theoretically goes to infinity—the most attractive property for applications. The applicability and benefits of optical BICs have already been demonstrated for various optical effects, such as lasing generation [12,13], sensing [14,15], magneto-optics [16], high harmonic generation [17], filtering [18], electrically driven transparency [19], photonic spin Hall effect [20], etc.

The two main types of optical BICs are symmetry-protected and accidental (Friedrich-Wintgen) BICs. The former originates from the symmetry mismatch between the resonant mode and external radiation and appears at highly symmetric points, such as the Γ point in the reciprocal space of the periodic structure. The latter is formed by the destructive interference between the radiation from the resonant

modes and can appear at a point of no symmetry in the reciprocal space.

In the early paper by Paddon [21], bound states above the vacuum light line were observed for the square-lattice dielectric photonic crystals slab. These states arise at the Brillouin zone regions, where dispersion curves of the guided modes overlap. Coupling of the guided modes leads to the bands' anticrossing. It is noteworthy that anticrossing and bound states appear not only for the modes with the same polarization (TE or TM) but also for the orthogonal modes. This peculiar property of the two-dimensional (2D) lattices provides additional flexibility for tuning of the BIC spectral position compared with the 1D structures.

The anticrossing of the dispersion curves is a well-known signature of the strong coupling between the modes [22]. This effect is familiar for systems in which plasmonic and photonic resonances interact. Strong coupling effects in plasmon-photon systems have been widely investigated in 1D structures with either surface or localized plasmon resonances [23–29].

Recently, it was shown that localized photonic modes (e.g., Mie modes) interacting via diffraction channels [13] or guided [30] modes form hybrid modes possessing BICs. Moreover, lasing generation has been achieved in such structures. Similar results have been demonstrated for structures with plasmonic surface lattice resonances lasing in dark modes [31], which also can be treated as BICs.

In this work, we present the study of the optical response of the 2D plasmonic array fabricated on the luminescent waveguide layer. Gold nanodisks arranged in a square lattice provided light coupling to both the TE and TM guided modes, while the size of a single nanodisk supports localized plasmon resonance rather than surface plasmon resonance. In addition, the influence of the eigenmodes' dispersion curves on the emitting properties of the structure is observed.

*Pavlov_Sergey@mail.ioffe.ru

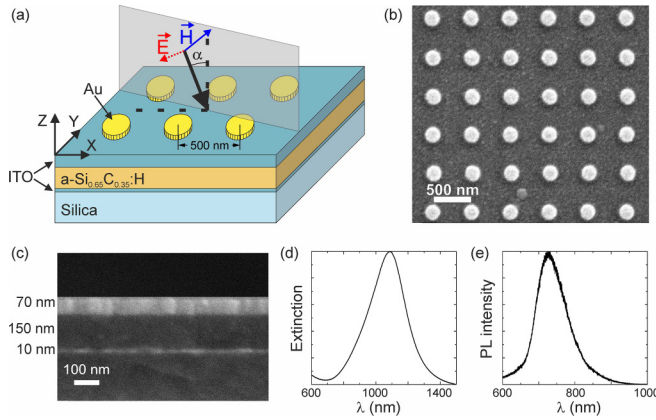


FIG. 1. (a) Schematic view of the structure. (b) SEM top view image of the 2D array of the gold nanodisks. (c) SEM cross-section image of the substrate with waveguide layers. (d) Calculated extinction spectrum of a single gold disk on the corresponding substrate. (e) Normalized PL intensity of the $a\text{-Si}_{0.65}\text{C}_{0.35}\text{:H}$ film.

II. STRUCTURE, EXPERIMENTAL, AND THEORETICAL METHODS

The schematic view of structure and scanning electron microscope (SEM) images of the experimental sample are shown in Figs. 1(a)–1(c). The waveguide layer consists of a 150-nm-thick $a\text{-Si}_{0.65}\text{C}_{0.35}\text{:H}$ film sandwiched between indium tin oxide (ITO) layers (10 nm and 70 nm) on the silica substrate. The 2D array of gold disks arranged in the square lattice with period $P = 500$ nm was created on top of the waveguide layer. The disk's size (thickness, 20 nm; diameter, 200 nm) provided LPR excitation with peak wavelength at ~ 1100 nm with a wide tail down to 800 nm [Fig. 1(d)]. The photoluminescence (PL) spectrum of the $a\text{-Si}_{0.65}\text{C}_{0.35}\text{:H}$ film without the gold structure exhibits peak maximum at 725 nm [Fig. 1(e)], which is in agreement with [32]. Details on the technological processes and optical properties of the materials used are given in the Supplemental Material [33] (Secs. I and II, respectively).

To examine the resonant modes of the structure we performed angle-resolved reflection and PL spectra measurements by the Fourier-imaging spectroscopy method using an Acton SP2500 monochromator in the range of 500–1100 nm. The angle range available in our experiment defined by the numerical aperture of the micro-objective used was about $\pm 40^\circ$. The emission was excited with a continuous-wave semiconductor laser at a wavelength of 405 nm (the corresponding photon energy exceeds the electronic energy gap width of $a\text{-Si}_{1-x}\text{C}_x\text{:H}$ at any value of x). The power density of laser light did not exceed $40 \text{ mW}/\text{mm}^2$. No PL signal was detected, either, from the silica substrates we used. The schematic of the experimental setup and details of the method were presented in our previous work [34].

Numerical calculations of the angle-resolved reflection and PL spectra of the structure were performed by a Fourier modal method in the scattering matrix form, also known as rigorous coupled-wave analysis [35]. Calculations of the structures' eigenmodes including dispersion relations, electromagnetic fields, and Q factors were performed by the finite element commercial software COMSOL MULTIPHYSICS.

III. RESULTS

A. Empty-lattice approximation

In order to understand the origin of the resonant modes we begin with the empty-lattice approximation of a slab waveguide as a first step. In the empty-lattice approximation the structure consists of waveguide layers without gold disks. Without periodic corrugation, the guided modes in a planar waveguide are bound modes, confined in the slab. Introduction of periodic conditions with period P is equivalent to the folding guided modes into the first Brillouin zone. These folded guided modes are shown in Fig. 2(a). The particular modes can be explained by considering 2D diffraction by a square lattice [Figs. 2(b) and 2(c)].

To be specific, we assume s -polarized light incident on the structure in the x - z plane (electric field \mathbf{E} is parallel to the y axis) at an angle α . Light diffracted by a periodic structure couples to guided modes at the energy-momentum conservation conditions: $2\pi c/\lambda = \omega_{wg}$ and $|\mathbf{k}_{\text{dif}}| \equiv |\mathbf{k}_{\parallel} + \mathbf{G}| = \beta$, where ω_{wg} and β are the angular frequency and propagation constant of the guided mode, $\mathbf{k}_{\parallel} = k_0 \sin \alpha$ is the wave vector component parallel to the surface, λ and k_0 are the wavelength and wave vector of the incident light, $\mathbf{G} = (m_x \mathbf{b}_x, m_y \mathbf{b}_y)$ is the reciprocal lattice vector, $\mathbf{b}_x = \mathbf{b}_y = 2\pi/P$ are the reciprocal lattice primitive vectors, and m_i are the integers. Hereafter we represent diffraction by \mathbf{G} with the two values (m_x, m_y) .

At oblique incidence, $(\pm 1, 0)$ diffraction couples light to TE guided modes propagating along the x axis in opposite directions, yet with the different frequencies. At the same time, $(0, \pm 1)$ diffraction couples light to TE modes propagating in mirror with respect to x axis directions as depicted in Fig. 2(b). Since $|\mathbf{k}_{\text{dif}}|$ for both $(0, \pm 1)$ orders are equal, these modes are degenerate. At normal incidence $|\mathbf{k}_{\text{dif}}|$ for all $(\pm 1, 0)$ and $(0, \pm 1)$ diffraction orders are equal; thus the TE-guided modes at the Γ point are fourfold degenerate.

For the light, incident in the Γ - M direction (45° to the x axis), the pairs of $(1, 0)/(0, 1)$ and $(-1, 0)/(0, -1)$ diffractions give pairs of doubly degenerate TE modes propagating in mirror with respect to \mathbf{k}_{\parallel} [Fig. 2(c)].

The foregoing allows one to instantly explain the remaining modes in Fig. 2(b). The modes labeled as TM arise from p -polarized light and TM-guided modes and the modes labeled as TE' and TM' are from diffraction on 45° -rotated lattice with $\mathbf{G}' = \sqrt{2}\mathbf{G}$ and thus exchange Γ - X and Γ - M directions.

In addition, we notice that the only guided modes propagating along incident light direction have corresponding polarization, so these modes cannot be excited by the orthogonally polarized light. For example, TE $(\pm 1, 0)$ modes cannot be excited by the p -polarized light in the Γ - X direction, while TE $(0, \pm 1)$ can.

Summing up we have quartets of TE (TM) modes fourfold degenerate at the Γ point that are split into two singlets and one doublet in the Γ - X direction and two doublets in the Γ - M direction.

Under the illumination of the periodically modulated structure, light can couple to guided modes, which causes the appearance of the resonant features in the spectra. These features follow the dispersion curves of the guided modes and, in general, have Fano line shapes.

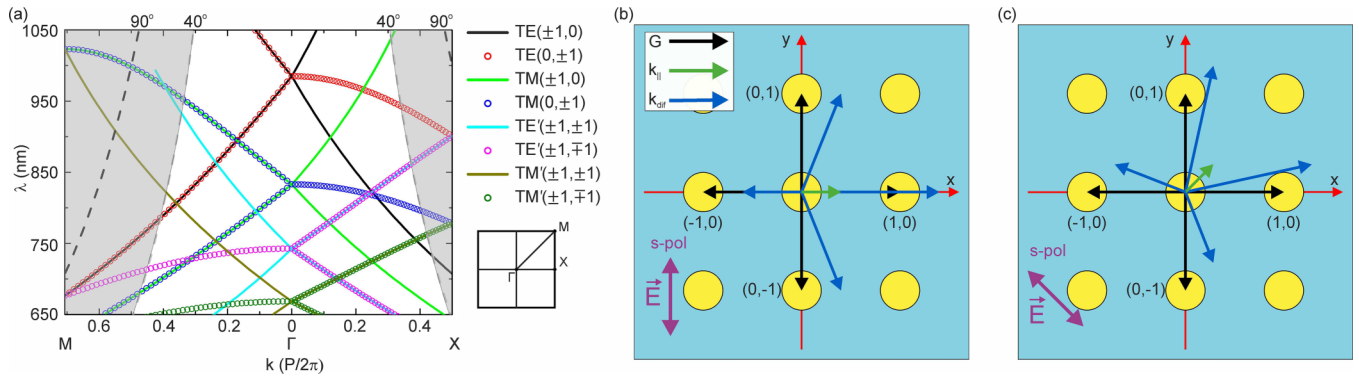


FIG. 2. (a) Eigenmodes of the structure in empty-lattice approximation. Shaded regions depict angular ranges unavailable in the experiment; dashed lines are referred to as the light line, which shows the dispersion relation in air. (b) Schematic of the light diffraction on the square lattice for the light incident in the Γ - X direction. (c) The same as (b) but for the light incident in the Γ - M direction.

Though the empty-lattice approximation describes the spectral position of the resonances quite well, it cannot explain mode splitting and shift caused by the mode interaction, as well as the bound states formation. This requires rigorous eigenmodes' analysis of the corrugated structure.

B. Effect of the plasmonic nanodisks

Next, we take into account the presence of the gold nanodisks and thus the localized plasmon excitation. Interaction between the electric fields of the guided modes and the localized plasmon leads to the formation of the hybrid guided-plasmon modes and, as a result, lifts the degeneracy. The fundamental property of a square lattice symmetry C_{4v} is the existence of two degenerate and two nondegenerate states at the Γ point [36]. The calculated eigenmodes' dispersion of

the structure in Fig. 3(a) shows that each fourfold degenerate quartet splits into nondegenerate states of higher wavelengths and doubly degenerate states at lower wavelengths. In the Γ - X and Γ - M directions symmetry lowers to C_{1h} and thus all modes become nondegenerate.

According to [21,37] we can determine the symmetry of each mode by examining the spatial distribution of its electric field z component. Calculated field distributions for the upper TE quartet are presented in Fig. 3(b) (the others are shown in the Supplemental Material [33], Sec. III). From these pictures it is seen that at the Γ point mode 1 corresponds to the B_2 , mode 2 to the A_2 , and modes 3 and 4 to the E irreducible representation of point group C_{4v} , respectively (see Table I).

In the Γ - X direction modes 1, 2, and 4 (as well as 7, 10, and 12) are antisymmetric under mirror reflection operation around the x axis, while mode 3 (and also 5, 6, 8, 9, and

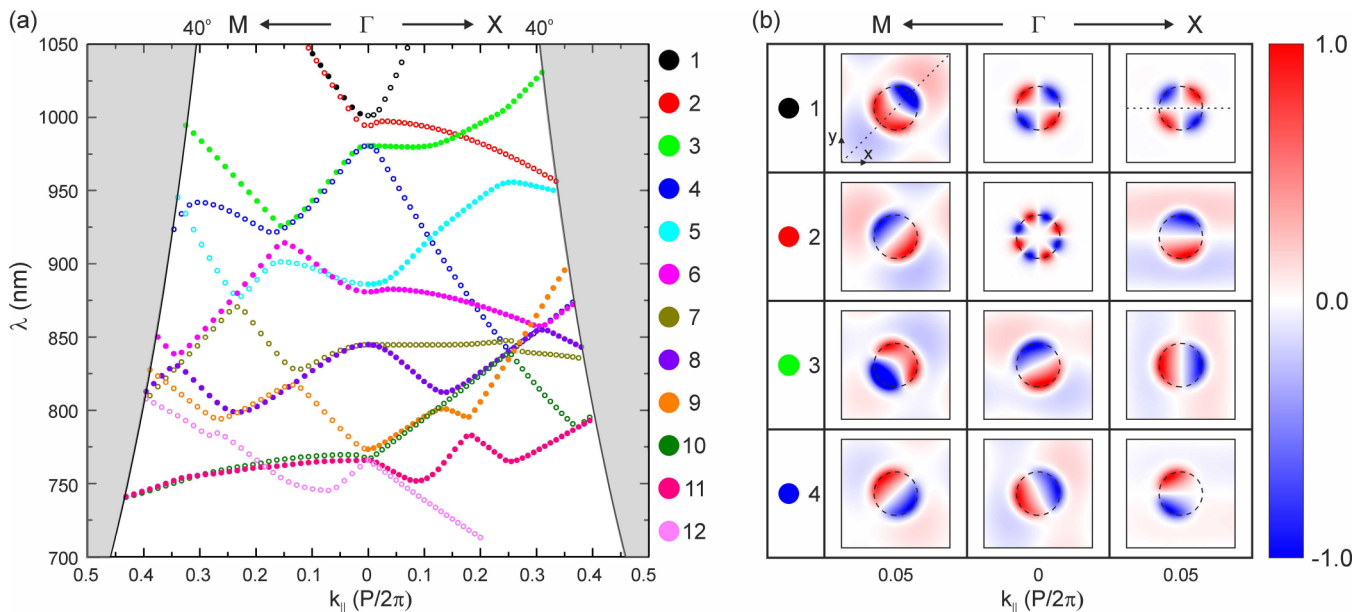


FIG. 3. (a) Calculated eigenmodes dispersion of the structure. Solid circles denote the modes that are symmetric relative to the corresponding direction; hollow circles denote the antisymmetric ones. (b) Electric field z -component distributions in the x - y plane of the unit cell for the upper TE quartet. The fields are calculated in the Γ point and at the $k_{||} = 0.05P/2\pi$ in the Γ - X and Γ - M directions. The contour of the gold nanodisks is shown with a black dashed circle. The black dotted lines in the upper row depict axes of the symmetry in the corresponding directions.

TABLE I. Character table for the C_{4v} and C_{1h} point groups.

C_{4v}	E	$2C_4$	C_2	$2\sigma_v$	$2\sigma_d$
A_1	1	1	1	1	1
A_2	1	1	1	-1	-1
B_1	1	-1	1	1	-1
B_2	1	-1	1	-1	1
E	2	0	-2	0	0

C_{1h}	E	σ
A	1	1
B	1	-1

11) is symmetric. Thus the former modes can be denoted as s polarized (B irreducible representation of point group C_{1h}) and the latter as p polarized (A irreducible representation of point group C_{1h}), respectively. In the Γ - M direction one mode of higher wavelengths in each set changes its symmetry, while the others retain their symmetry (and should be treated relative to the diagonal of the cell).

These considerations explain the anticrossing between modes with the same symmetry even though they originate from the guided modes with orthogonal polarization. For example, one can see that in the Γ - X direction anticrossing occurs between modes 3 (originating from the TE mode) and 5 (originating from the TM mode), while these modes cross modes 2 and 4, respectively, without any interaction. At the same time in the Γ - M direction mode 5 changes its symmetry and hence interacts with mode 4.

Angle-resolved reflectance spectra maps of the structure described in Sec. II are presented in Fig. 4. The resonances associated with the eigenmodes of the structure excitation appear as reflection minima lines in the reflectance maps. It should be noted that additional lines are observed in the experimental spectra, which arise from misalignment of sample

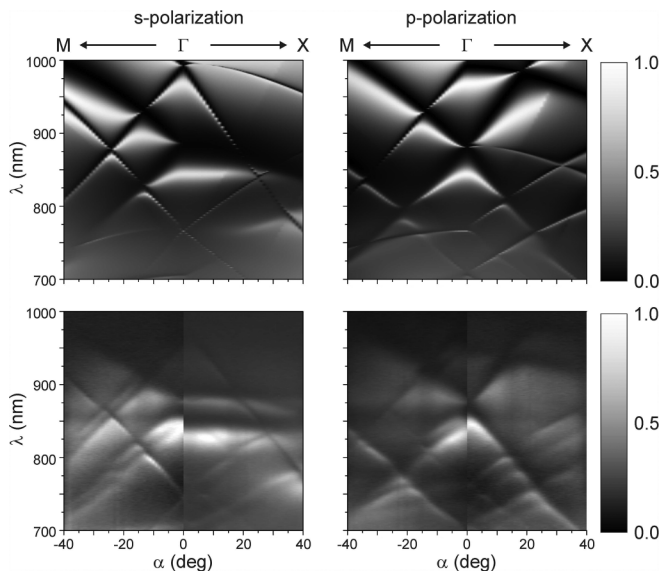


FIG. 4. Angle-resolved reflection spectra. Upper row: calculation; lower row: experiment.

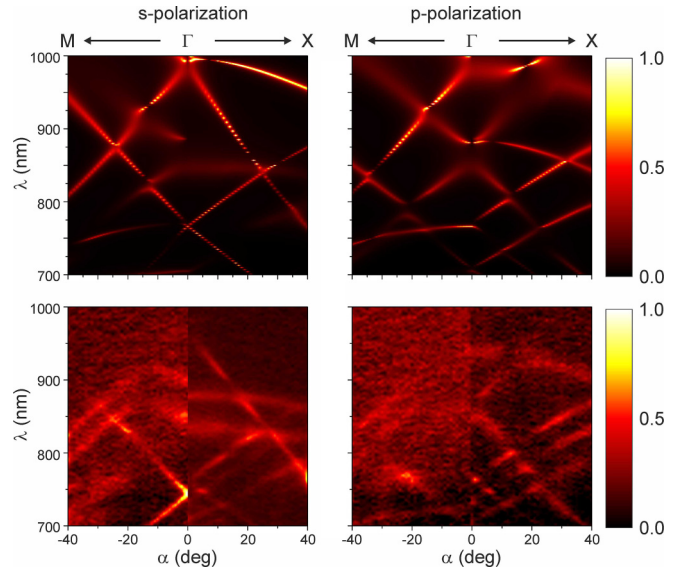


FIG. 5. Angle-resolved PL spectra. Upper row: calculation; lower row: experiment.

positioning in respect to the z axis, which is not accounted for in calculations. Also, the deviation of the calculations and experimental results in the long-wavelength range (900–1000 nm) may arise because of discrepancy of the optical constants of the materials used in calculations. Despite these deviations, we believe that our experimental measurements are in reasonable agreement with the calculated ones, which proves their analysis.

The resonances observed in the reflectance maps exhibit qualitative agreement with the eigenmodes' dispersion curves. However, the width of some resonance lines does not allow the modes' splitting and anticrossing to be clearly observed. This resonance broadening arises because of the strong interaction between the plasmonic mode with guided modes with appropriate polarization. This can be easily understood considering again empty-lattice approximation. Under the p -polarized incident light, the electric field of the localized plasmon is directed along the axis of incidence. Thus it can strongly interact with guided modes the electric field of which is directed in the same way. These are, for example, TE $(0, \pm 1)$ and TM $(\pm 1, 0)$ guided modes in the Γ - X direction. At the same time the electric field of the TM $(0, \pm 1)$ guided mode is oriented mainly along the y axis and the interaction between this guided mode and the plasmonic one is suppressed. Thus the width of this resonance line is much narrower.

To reveal the influence of the eigenmodes on the optical response we performed PL measurements and calculations of the emissivity of the structure (Fig. 5). The obtained angle-resolved PL spectra maps coincide with the reflectance ones, while narrower emission resonance linewidths in comparison with the reflectance allow us to observe resonance modes splitting and anticrossing. The most pronounced splitting is observed at the normal incidence in the 850 nm region, which is consistent with calculations in Fig. 3(a).

In addition, the vanishing of the emission lines at certain points is clearly observed. Vanishing of the emission means that light generated in the α - $\text{Si}_{0.65}\text{C}_{0.35}\text{:H}$ layer does not

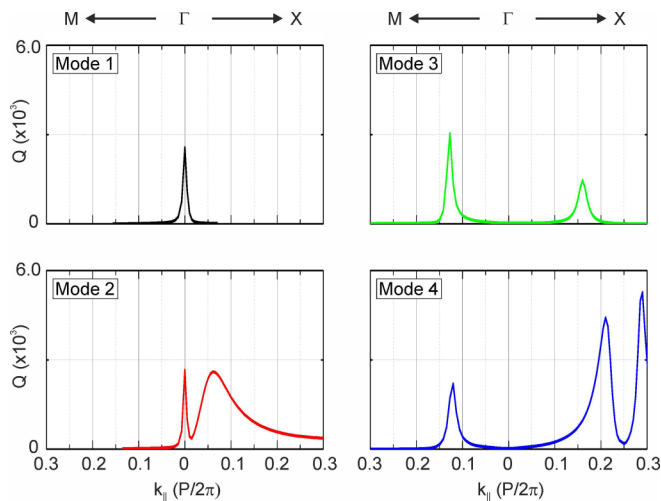


FIG. 6. Calculated Q -factor dependencies for the eigenmodes presented in Fig. 3.

outcouple to free space. At the same time, one can observe a significant increase in the emissivity intensity near the vanishing points (for instance, the point at 20° and 990 nm in the calculated p -polarization map Fig. 5). This behavior may indicate the formation of the bound state.

C. Bound states in the continuum

Anticrossing behavior is a clear evidence of the coupling between modes. Near the anticrossing a bound polaritonic state may occur. In order to reveal this phenomenon we have calculated the Q -factor dependencies for the modes (Fig. 6). The obtained curves exhibit several peaks at different k points. At the Γ point there are peaks for the nondegenerate modes 1 and 2 (this is also true for the modes 5 and 6; see Supplemental Material [33], Sec. III). These states can be attributed to the well-known symmetry-protected BICs, since only the E modes in the photonic crystal couple to the external radiation field [38].

The second set with narrow linewidths in the k space appears at the off- Γ points near the modes' anticrossing. These are the peaks at about $k_{\parallel} = 0.15P/2\pi$ for mode 3 in the Γ - X direction (the point at 20° and 990 nm in the p -polarization map) and for the modes 3 and 4 in the Γ - M direction (the point at -15° and 925 nm in the p -polarization and s -polarization maps). These bound states arise due to polaritonic state formation and are referred as “accidental” Friedrich-Wintgen BICs.

Another peculiar feature appears as a rather wide peak in the mode 2 Q -factor dependence (and also for mode 6). This feature coincides with the vanishing of the corresponding resonant lines in the reflection and PL spectra (the points at 5° and 995 nm in the s -polarization map and at 5° and

880 nm in the p -polarization map). The resonant line behavior could indicate BIC though the Q -factor peak is too wide. This discrepancy arises because calculated Q include both radiative and nonradiative losses from material absorption. Therefore, the maximum Q values do not exceed $\sim 10^4$ even for well-defined symmetry-protected BICs. Contrary to the “polaritonic” BICs these BICs can be thought of as originating from destructive interference of the radiative components of the plasmonic and guided resonances. This assumption seems to be valid due to the results obtained for the modes 9–12 that arise from TE' guided modes (see Sec. III A). These modes lie at the wavelength region where plasmonic excitation is low; thus interaction between quasiguided and plasmonic modes is negligible. As a result there is no BIC formation and no resonant lines vanishing are observed in reflection and PL spectra. Since each eigenmode in the region above ~ 800 nm is hybridized from pure guided and plasmonic modes, one can call these bound states “single-mode” BICs.

IV. CONCLUSIONS

In this work, we have studied the optical properties of the structure consisting of the waveguide luminescent layer covered by the 2D plasmonic array. We have shown that resonances observed in the reflection and PL spectra originate from the TE and TM quasiguided modes hybridized with the localized plasmonic modes. Gold disks arranged in a square lattice provide BICs formation of the three types—symmetry-protected, polaritonic, and “single-mode” BICs. Symmetry-protected BICs are the most common effect of the photonic structures possessing specific symmetry. Points at which these types of BICs are present can be rigorously predicted by the group theory. Polaritonic BICs arise in the vicinity of the modes anticrossing, which is the evidence of the polaritonic state formation. In contrary with the above stated BICs, the so-called single-mode BIC is observed at a point where no modes' anticrossing or specific symmetry is present. We believe that this bound state is due to the interference of propagating and localized resonances. In our case these resonances are the quasiguided and plasmonic ones.

Though the Q factor of the BICs in the structures with plasmonic elements is rather low compared with the full-dielectric devices, the results of this study can pave the way for further research of the BIC formation in the systems combining collective and single-particle resonances.

ACKNOWLEDGMENTS

The experimental part of this work was supported in the framework of the state budget agreement (No. 0040-2019-0012).

- [1] S. Pandey, N. Baburaj, S. Joseph, and J. Joseph, Resonant optical modes in periodic nanostructures, *ISSS J. Micro Smart Syst.* **11**, 113 (2022).
- [2] K. Yang, X. Yao, B. Liu, and B. Ren, Metallic plasmonic array structures: Principles, fabrications, properties, and applications, *Adv. Mater.* **33**, 2007988 (2021).

- [3] V. Amendola, R. Pilot, M. Frascioni, O. M. Maragò, and M. A. Iatì, Surface plasmon resonance in gold nanoparticles: A review, *J. Phys.: Condens. Matter* **29**, 203002 (2017).
- [4] R. Guo, T. K. Hakala, and P. Törmä, Geometry dependence of surface lattice resonances in plasmonic nanoparticle arrays, *Phys. Rev. B* **95**, 155423 (2017).

- [5] V. G. Kravets, A. V. Kabashin, W. L. Barnes, and A. N. Grigorenko, Plasmonic surface lattice resonances: A review of properties and applications, *Chem. Rev.* **118**, 5912 (2018).
- [6] R. Collison, J. B. Pérez-Sánchez, M. Du, J. Trevino, J. Yuen-Zhou, S. O'Brien, and V. M. Menon, Purcell effect of plasmonic surface lattice resonances and its influence on energy transfer, *ACS Photon.* **8**, 2211 (2021).
- [7] A. D. Utyushev, V. I. Zakomirnyi, and I. L. Rasskazov, Collective lattice resonances: Plasmonics and beyond, *Rev. Phys.* **6**, 100051 (2021).
- [8] S. G. Tikhodeev, A. L. Yablonskii, E. A. Muljarov, N. A. Gippius, and T. Ishihara, Quasiguidded modes and optical properties of photonic crystal slabs, *Phys. Rev. B* **66**, 045102 (2002).
- [9] S. A. Dyakov, N. A. Gippius, M. M. Voronov, S. A. Yakovlev, A. B. Pevtsov, I. A. Akimov, and S. G. Tikhodeev, Quasiguidded modes of opaline photonic crystals covered by Ge₂Sb₂Te₅, *Phys. Rev. B* **96**, 045426 (2017).
- [10] C. W. Hsu, B. Zhen, A. D. Stone, J. D. Joannopoulos, and M. Soljacic, Bound states in the continuum, *Nat. Rev. Mater.* **1**, 16048 (2016).
- [11] S. I. Azzam and A. V. Kildishev, Photonic bound states in the continuum: From basics to applications, *Adv. Opt. Mater.* **9**, 2001469 (2021).
- [12] A. Kodigala, T. Lepetit, Q. Gu, B. Bahari, Y. Fainman, and B. Kanté, Lasing action from photonic bound states in continuum, *Nature (London)* **541**, 196 (2017).
- [13] S. T. Ha, Y. H. Fu, N. K. Emani, Z. Pan, R. M. Bakker, R. Paniagua-Domínguez, and A. I. Kuznetsov, Directional lasing in resonant semiconductor nanoantenna arrays, *Nat. Nanotechnol.* **13**, 1042 (2018).
- [14] S. Romano, G. Zito, S. N. L. Yépez, S. Cabrini, E. Penzo, G. Coppola, I. Rendina, and V. Mocellaark, Tuning the exponential sensitivity of a bound-state-in-continuum optical sensor, *Opt. Express* **27**, 18776 (2019).
- [15] F. Wu, J. Wu, Z. Guo, H. Jiang, Y. Sun, Y. Li, J. Ren, and H. Chen, Giant enhancement of the goos-hänchen shift assisted by quasibound states in the continuum, *Phys. Rev. Appl.* **12**, 014028 (2019).
- [16] V. A. Zakharov and A. N. Poddubny, Transverse magneto-optical kerr effect enhanced at the bound states in the continuum, *Phys. Rev. A* **101**, 043848 (2020).
- [17] T. Ning, X. Li, Y. Zhao, L. Yin, Y. Huo, L. Zhao, and Q. Yue, Giant enhancement of harmonic generation in all-dielectric resonant waveguide gratings of quasi-bound states in the continuum, *Opt. Express* **28**, 34024 (2020).
- [18] J. M. Foley, S. M. Young, and J. D. Phillips, Symmetry-protected mode coupling near normal incidence for narrow-band transmission filtering in a dielectric grating, *Phys. Rev. B* **89**, 165111 (2014).
- [19] J. Li, J. Li, C. Zheng, Z. Yue, S. Wang, M. Li, H. Zhao, Y. Zhang, and J. Yao, Free switch between bound states in the continuum (bic) and quasi-bic supported by graphene-metal terahertz metasurfaces, *Carbon* **182**, 506 (2021).
- [20] F. Wu, T. Liu, Y. Long, S. Xiao, and G. Chen, Giant photonic spin hall effect empowered by polarization-dependent quasibound states in the continuum in compound grating waveguide structures, *Phys. Rev. B* **107**, 165428 (2023).
- [21] P. Paddon and J. F. Young, Two-dimensional vector-coupled-mode theory for textured planar waveguides, *Phys. Rev. B* **61**, 2090 (2000).
- [22] P. Törmä and W. L. Barnes, Strong coupling between surface plasmon polaritons and emitters: A review, *Rep. Prog. Phys.* **78**, 013901 (2014).
- [23] A. Christ, S. G. Tikhodeev, N. A. Gippius, J. Kuhl, and H. Giessen, Waveguide-plasmon polaritons: Strong coupling of photonic and electronic resonances in a metallic photonic crystal slab, *Phys. Rev. Lett.* **91**, 183901 (2003).
- [24] A. Christ, T. Zentgraf, J. Kuhl, S. G. Tikhodeev, N. A. Gippius, and H. Giessen, Optical properties of planar metallic photonic crystal structures: Experiment and theory, *Phys. Rev. B* **70**, 125113 (2004).
- [25] S. I. Azzam, V. M. Shalaev, A. Boltasseva, and A. V. Kildishev, Formation of bound states in the continuum in hybrid plasmonic-photonic systems, *Phys. Rev. Lett.* **121**, 253901 (2018).
- [26] S. Dyakov, D. Zhigunov, A. Marinins, O. Shalygina, P. Vabishchevich, M. Shcherbakov, D. Presnov, A. Fedyanin, P. Kashkarov, S. Popov, N. Gippius, and S. Tikhodeev, Plasmon induced modification of silicon nanocrystals photoluminescence in presence of gold nanostructures, *Sci. Rep.* **8**, 4911 (2018).
- [27] R. Kikkawa, M. Nishida, and Y. Kadoya, Polarization-based branch selection of bound states in the continuum in dielectric waveguide modes anti-crossed by a metal grating, *New J. Phys.* **21**, 113020 (2019).
- [28] R. Kikkawa, M. Nishida, and Y. Kadoya, Bound states in the continuum and exceptional points in dielectric waveguide equipped with a metal grating, *New J. Phys.* **22**, 073029 (2020).
- [29] S. Joseph, S. Sarkar, S. Khan, and J. Joseph, Exploring the optical bound state in the continuum in a dielectric grating coupled plasmonic hybrid system, *Adv. Opt. Mater.* **9**, 2001895 (2021).
- [30] M. Wu, L. Ding, R. P. Sabatini, L. K. Sagar, G. Bappi, R. Paniagua-Domínguez, E. H. Sargent, and A. I. Kuznetsov, Bound state in the continuum in nanoantenna-coupled slab waveguide enables low-threshold quantum-dot lasing, *Nano Lett.* **21**, 9754 (2021).
- [31] T. K. Hakala, H. T. Rekola, A. I. Väkeväinen, J.-P. Martikainen, M. Nečada, A. J. Moilanen, and P. Törmä, Lasing in dark and bright modes of a finite-sized plasmonic lattice, *Nat. Commun.* **8**, 13687 (2017).
- [32] B. Akaoglu, K. Sel, I. Atilgan, and B. Katircioglu, Carbon content influence on the optical constants of hydrogenated amorphous silicon carbon alloys, *Opt. Mater. (Amsterdam)* **30**, 1257 (2008).
- [33] See Supplemental Material at <http://link.aps.org/supplemental/10.1103/PhysRevB.108.205425> for details on the sample fabrication processes, optical properties of the materials, calculated electric field distributions, and q factors for all presented eigenmodes.
- [34] S. I. Pavlov, S. A. Dyakov, A. I. Solomonov, A. V. Nashchekin, N. A. Feoktistov, N. A. Gippius, S. G. Tikhodeev, A. K. Samusev, and A. B. Pevtsov, Eigenmode analysis of the waveguide-plasmon structure based on a-si1-xcx:h layer with 1d gold grating, *Photon. Nanostruct. Fundam. Appl.* **48**, 100975 (2022).

- [35] M. G. Moharam, E. B. Grann, D. A. Pommet, and T. K. Gaylord, Formulation for stable and efficient implementation of the rigorous coupled-wave analysis of binary gratings, *J. Opt. Soc. Am. A* **12**, 1068 (1995).
- [36] K. Sakoda, *Optical Properties of Photonic Crystals*, 2nd ed., Springer Series in Optical Sciences (Springer, Berlin, Heidelberg, 2005).
- [37] J. Lee, B. Zhen, S.-L. Chua, W. Qiu, J. D. Joannopoulos, M. Soljačić, and O. Shapira, Observation and differentiation of unique high- q optical resonances near zero wave vector in macroscopic photonic crystal slabs, *Phys. Rev. Lett.* **109**, 067401 (2012).
- [38] T. Ochiai and K. Sakoda, Dispersion relation and optical transmittance of a hexagonal photonic crystal slab, *Phys. Rev. B* **63**, 125107 (2001).